

# Diversity Analysis for Terahertz Communication Systems under Small-Scale Fading

Almutasem Bellah Enad<sup>†</sup>, Jihad Fahs<sup>†</sup>, Hakim Jemaa<sup>\*</sup>, Hadi Sarieddeen<sup>†</sup>, Tareq Y. Al-Naffouri<sup>\*</sup>

<sup>†</sup>Department of Electrical and Computer Engineering, American University of Beirut, Beirut, Lebanon,

<sup>\*</sup>Department of Computer, Electrical and Mathematical Sciences and Engineering, KAUST, Kingdom of Saudi

Email: {aae118, jihad.fahs, hadi.sarieddeen}@aub.edu.lb, {hakim.jemaa, tareq.alnaffouri}@kaust.edu.sa

**Abstract**—The terahertz (THz) band is a key enabler for future wireless systems, promising ultra-high data rates and dense spatial reuse. However, the reliability of THz links remains a major challenge due to severe path loss and small-scale fading effects, particularly in dynamic indoor and outdoor environments. This paper presents a comprehensive diversity analysis framework for THz communication systems under realistic small-scale fading conditions. We model fading statistically using the generalized  $\alpha$ - $\mu$  distribution for indoor scenarios and the mixture of gamma (MG) model for outdoor propagation. We complement previous works that analyzed diversity under  $\alpha$ - $\mu$  channels [1], [2]. In particular, we present new insights on diversity for the MG channel in addition to recovering the results of [2] using a different approach. Moreover, we derive asymptotic expressions for the bit error rate as a function of the inverse signal-to-noise ratio, recovering all of the  $\alpha$ - $\mu$  diversity results using a simpler approximation method. The analytical results are extensively validated through Monte Carlo simulations, demonstrating excellent agreement. Our findings show that the achievable diversity in THz systems is strongly influenced by the number of independent paths, the severity of fading, and frequency selectivity. The proposed framework provides system designers with clear guidelines to quantify and optimize diversity gains under emerging channel models, paving the way for more reliable high-frequency wireless links in next-generation networks.

**Index Terms**—THz communications, bit-error probability, diversity,  $\alpha$ - $\mu$  distribution, mixture of gamma distribution.

## I. INTRODUCTION

The terahertz (THz) band, spanning 100 GHz to 10 THz, is poised to enhance future wireless systems by enabling ultra-high data rates in the terabit-per-second range and supporting extremely low-latency communications [3]. These capabilities are essential for emerging applications such as real-time holographic communication, high-resolution sensing, and ultra-reliable machine-type communication [3]. Despite these promises, THz propagation faces unique physical challenges. Recent studies reveal that THz signals exhibit significant temporal and spatial sparsity [4], [5], yet can still support non-line-of-sight (NLoS) communication under favorable conditions [4]. However, in practice- even in indoor environments- the availability of NLoS paths is limited and becomes further constrained under high-gain directional antennas [5], which are often necessary to overcome severe path loss. In this context,

This work is supported by the AUB's University Research Board and Vertically Integrated Projects Program, and KAUST's Office of Sponsored Research under Award No. ORFS-CRG12-2024-6478.

accurately characterizing small-scale fading becomes critical for ensuring link reliability and efficient resource allocation. Measurement-based analyses have shown that the generalized  $\alpha$ - $\mu$  distribution offers a robust statistical model for describing small-scale fading behavior in indoor THz channels [6], making it a powerful tool for performance prediction and system design. Unlike classical fading models such as the Nakagami- $m$  and Rician distributions, which often fall short in capturing the complex and highly correlated nature of THz propagation, the  $\alpha$ - $\mu$  model provides a flexible and accurate parameterization tailored for such environments [7]. Its versatility has proven effective in building analytical frameworks for indoor THz communication, notably when combined with misalignment fading effects modeled via the zero-boresight approach [8]. These enhancements are critical for supporting reliable beamforming and alignment strategies in dense future network deployments. On the other hand, the mixture of gamma (MG) distribution, originally introduced for symbol error analysis in conventional wireless systems [9], has been successfully applied to characterize diversity reception over generalized- $K$  fading channels [10]. Its ability to approximate a wide range of fading conditions makes it a strong candidate for modeling outdoor THz channels with complex multipath structures in next-generation networks. A recent study presented a comprehensive performance analysis framework for outdoor THz SISO channels under MG fading with beam misalignment effects [11], highlighting the growing interest in accurate statistical modeling for THz environments.

Diversity techniques remain indispensable for enhancing the robustness and reliability of wireless links [12]. This is particularly true for THz communication systems, where severe path loss, molecular absorption, and small-scale fading significantly degrade link performance [3]. Exploiting spatial, frequency, and polarization diversity [12], [13] can effectively mitigate these impairments and counteract the limited multipath richness typical of high-frequency channels.

In this paper, we study the  $L$ -order diversity assuming a maximum ratio combiner (MRC) receiver. We provide a detailed analysis for realistic THz channels, where the fading is modeled as MG and two variants of  $\alpha$ - $\mu$  distributions for outdoor and indoor, respectively. The main contributions of this paper are summarized as follows:

- For the indoor THz scenario, we propose the use of a simplified approximation method [12] for evaluating the

diversity order. Our analysis yields results consistent with those in [1], [2], while offering a more mathematically tractable and intuitive derivation compared to the exact methods used in these references. For the second  $\alpha\text{-}\mu$  model, we provide yet another approach to recover the results of [2].

- For the outdoor case, and to the best of the authors' knowledge, this is the first work to analyze the error probability under a realistic outdoor THz system model. The derivation is carried out using the moment generating function (MGF) approach.

The proposed approximation method provides a smooth and tractable alternative to exact methods, enabling easier derivation and clearer mathematical insight while maintaining high accuracy. We show that  $\text{Pr}_e(\text{SNR}) = \Theta(\text{SNR}^{-\kappa_2}) = \kappa_1 \text{SNR}^{-\kappa_2} + o(\text{SNR}^{-\kappa_2})$ , where  $\kappa_2 = \frac{\alpha\mu}{2}L$  in the first  $\alpha\text{-}\mu$  model, recovering the result of [1], and  $\kappa_2 = \frac{\alpha}{2}\sum_{i=1}^L\mu_i$  in the second  $\alpha\text{-}\mu$  model, recovering the result of [2]. For the MG scenario, we find that  $\kappa_2 = (\frac{L}{2})\max_{1\leq j\leq N}\beta_j$ , where  $N$  is the number of mixtures. We also determine the multiplicative constant,  $\kappa_1$ . Throughout the paper, the  $|\cdot|$  operator represents the absolute value,  $\mathbb{E}[\cdot]$  is the expectation operator, and  $\text{Pr}(\cdot)$  is the probability operator.  $\Gamma(\cdot)$  is the gamma function.  $Q(x) = \frac{1}{\sqrt{2\pi}}\int_x^\infty e^{-\frac{u^2}{2}}du$  is the  $Q$ -function and  $\text{erf}(x) = \frac{2}{\sqrt{\pi}}\int_0^x e^{-u^2}du$  is the error function [14].  $H_{p,q}^{m,n}\left[z\left|\begin{matrix}(a_1,b_1),\dots,(a_p,b_p) \\ (c_1,d_1),\dots,(c_p,d_p) \end{matrix}\right.\right]$  represents the Fox H-function [15, eq. (1.1.1)]. We adopt the following conventions: for two asymptotically positive functions,  $f(x) = o(g(x))$  if for every  $c > 0$ ,  $f(x) \leq cg(x)$  for  $x$  large enough. We write  $f(x) = O(g(x))$  if there exists  $c > 0$  such that  $f(x) \leq cg(x)$  for  $x$  large enough.

## II. SYSTEM AND CHANNEL MODELS

We consider a single input, multiple output (SIMO) single carrier THz link with a complex baseband equivalent received signal for  $L \geq 1$  receiver's antenna [11],

$$\mathbf{r} = \mathbf{h}x + \mathbf{n}, \quad (1)$$

where  $\mathbf{r} = [r_1, \dots, r_L]^T$  is the received vector,  $x$  is the modulated transmitted symbol,  $\mathbf{n} = [n_1, \dots, n_L]^T$  is an additive white Gaussian noise with power  $N_0/2$  ( $N_0$  is the spectral density of the one-sided noise power) [16], and  $\mathbf{h} = [h_1, \dots, h_L]^T$  represents the overall channel fading vector with independent entries which is assumed independent of  $\mathbf{n}$ . Let  $v = \sqrt{P_t G_t G_r} h_p$ , then, each  $h_i$ ,  $1 \leq i \leq L$ , is defined as  $h = vh_f$ , where  $h_f$  is the complex small-scale fading and  $h_p$  represents the THz-band free-space path loss, consisting of both spreading and molecular absorption losses, expressed as [5]  $h_p = (c/4\pi fd)^{\frac{\varrho}{2}} e^{-K_{\text{abs}}d/2}$ , where  $c$  is the speed of light,  $f$  is the operating frequency,  $d$  is the communication distance, and  $K_{\text{abs}}$  is the molecular absorption coefficient (more details in [5]). In measurement-based sub-THz/THz works [5], [7], the path loss exponent,  $\varrho$ , is best-fit to 2.  $P_t$  denotes the transmit power, and  $G_t$  and  $G_r$  represent the gains of the transmit and receive antennas, respectively. For indoor THz channels,

we use the  $\alpha\text{-}\mu$ -distribution to represent the magnitude of  $h_f$ , where its PDF is expressed as [17]

$$f_{|h_f|}(y) = \frac{\alpha\mu^\mu y^{\alpha\mu-1}}{\hat{Z}^{\alpha\mu}\Gamma(\mu)} \exp(-\mu y^\alpha/\hat{Z}^\alpha), \quad (2)$$

where  $\alpha > 0$  is a fading parameter,  $\mu$  is the normalized variance of the fading channel, and  $\hat{Z} = \sqrt[\alpha]{\mathbb{E}(|h_f|^\alpha)}$  is the  $\alpha$  root mean value of the fading channel. Using (2), the PDF of  $h = vh_f$  can thus be expressed as

$$f_{|h|}(y) = \frac{1}{|v|} f_{|h_f|}\left(\frac{y}{v}\right) = \frac{\alpha\mu^\mu y^{\alpha\mu-1}}{(\hat{Z}v)^{\alpha\mu}\Gamma(\mu)} \exp(-\mu y^\alpha/(v\hat{Z})^\alpha), \quad (3)$$

which gives

$$f_{|h|^2}(y) = \frac{\alpha\mu^\mu}{2(\hat{Z}v)^{\alpha\mu}\Gamma(\mu)} y^{\frac{\alpha\mu}{2}-1} \exp\left(-\mu y^{\alpha/2}/(v\hat{Z})^\alpha\right). \quad (4)$$

Another parameterized form of the  $\alpha\text{-}\mu$  distribution is presented in [2],

$$f_{|h_f|}(x) = \frac{\alpha\beta^{\alpha\mu}}{\bar{x}^{\alpha\mu}\Gamma(\mu)} x^{\alpha\mu-1} \exp\left(-\left(\beta\frac{x}{\bar{x}}\right)^\alpha\right), \quad (5)$$

where  $\bar{x} = E\{h_f\}$  is the average of  $h_f$  and  $\beta = \frac{\Gamma(\mu+\frac{1}{\alpha})}{\Gamma(\mu)}$ . By applying a similar derivation to that used for (2), the PDF of  $|h|^2$  based on (5) is obtained as

$$f_{|h|^2}(y) = \frac{\alpha\beta^{\alpha\mu}}{2(\bar{x}v)^{\alpha\mu}\Gamma(\mu)} y^{\frac{\alpha\mu}{2}-1} \exp\left(-\left(\beta\frac{\sqrt{y}}{\bar{x}v}\right)^\alpha\right). \quad (6)$$

The two PDF forms of the  $\alpha\text{-}\mu$  distribution enable different analytical approaches and use cases, as detailed in the following sections.

For the outdoor THz model, the small-scale fading is modeled as a MG distribution [18], [19] whose PDF is expressed as [18]

$$f_{|h_f|}(y) = \sum_{i=1}^N w_i \frac{\zeta_i^{\beta_i} y^{\beta_i-1} e^{-\zeta_i y}}{\Gamma(\beta_i)} = \sum_{i=1}^N \alpha_i y^{\beta_i-1} e^{-\zeta_i y}, \quad y \geq 0, \quad (7)$$

where  $N$  is the number of gamma components, and  $\zeta_i$ ,  $\beta_i$  and  $w_i$  denote the scale, shape, and weight of the  $i$ th component where  $\sum_{i=1}^N w_i = 1$ . We define  $\alpha_i \triangleq w_i \zeta_i^{\beta_i} / \Gamma(\beta_i)$  for ease of notation. The PDF of  $|h|$  and  $|h|^2$  are given by

$$f_{|h|}(y) = \sum_{i=1}^N \frac{\alpha_i}{\sqrt{\beta_i}} y^{\beta_i-1} e^{-\frac{\zeta_i}{\sqrt{\beta_i}} y} \quad (8)$$

$$f_{|h|^2}(y) = \sum_{i=1}^N \frac{\alpha_i}{2\sqrt{\beta_i}} y^{\frac{\beta_i}{2}-1} e^{-\frac{\zeta_i}{\sqrt{\beta_i}} \sqrt{y}} \quad (9)$$

## III. PROBLEM FORMULATION

We consider an MRC receiver with perfect channel state information (CSI). The received signal is expressed as [12]

$$\tilde{r} = \frac{\mathbf{h}^*}{\|\mathbf{h}\|} \mathbf{r} = \frac{\mathbf{h}^*}{\|\mathbf{h}\|} (\mathbf{h}x + \mathbf{n}) = \|\mathbf{h}\| x + w, \quad (10)$$

where  $w = \frac{\mathbf{h}^*}{\|\mathbf{h}\|} \mathbf{n} \sim \mathcal{CN}(0, N_0)$ . We define the instantaneous signal-to-noise ratio (SNR) at the receiver, relative to the channel power, as

$$\gamma = \frac{E_s \|\mathbf{h}\|^2}{N_0} = \Upsilon \|\mathbf{h}\|^2, \quad \|\mathbf{h}\|^2 = \sum_{j=1}^L |h_j|^2, \quad (11)$$

where  $\Upsilon = \frac{E_s}{N_0}$ ,  $E_s$  is the energy per symbol, and each  $|h_j|^2$  is distributed either according to (4) or to (6). To analyze the diversity gain, we derive expressions for the bit error probability in the form  $\text{Pr}_e = \kappa_1 \Upsilon^{-\kappa_2} + o(\Upsilon^{-\kappa_2})$  in the high SNR

regime (high  $\Upsilon$ ), where  $\kappa_1, \kappa_2 > 0$ . To this end, we consider two approaches.

1- The first approach, proposed in [12], consists of approximating  $\Pr_e$  at high  $\Upsilon$  as

$$\Pr_e \approx \Pr\left(\|\mathbf{h}\|^2 \leq \frac{1}{\Upsilon}\right). \quad (12)$$

At high  $\Upsilon$ , the PDF of  $\|\mathbf{h}\|^2$  can be approximated for small values, enabling deriving approximate expressions for  $\Pr_e$ . We note that this method recovers the value of  $\kappa_2$  but fails to determine the exact value of  $\kappa_1$ .

2- The second approach is to compute the exact  $\Pr_e$  [13]:

$$\Pr_e = \mathbb{E}_{\|\mathbf{h}\|^2} \left[ Q\left(\sqrt{\Upsilon \|\mathbf{h}\|^2}\right) \right] = \int_0^\infty Q(\sqrt{\Upsilon x}) f_{\|\mathbf{h}\|^2}(x) dx. \quad (13)$$

This method fully characterizes  $\Pr_e$  as a function of  $\Upsilon$  and determines both  $\kappa_1$  and  $\kappa_2$ .

We note that both methods require knowledge of the PDF of  $\|\mathbf{h}\|^2$  as implied by (12) and (13).

#### IV. INDOOR DIVERSITY ANALYSIS

In this section, we provide expressions of the probability of error,  $\Pr_e$ , using both methods as outlined in Section III. The analysis is carried out for the THz indoor channel models given by (4) and (6).

##### A. The First $\alpha$ - $\mu$ Model

The diversity analysis for the  $\alpha$ - $\mu$  indoor channel model (3) is presented in [1] where it is found that

$$\Pr_{e \rightarrow \infty} = \left( \frac{\bar{\alpha} \mu^\mu \Gamma(\bar{\alpha} \mu)}{\Gamma(\mu) \bar{Z}^{\bar{\alpha} \mu}} \right)^L \frac{2^{-\varphi_0} \Gamma(\varphi_0 + \frac{1}{2})}{\Gamma(\varphi_0 + 1) \sqrt{\pi}} \Upsilon^{-\varphi_0} + o(\Upsilon^{-\varphi_0}), \quad (14)$$

where  $\bar{\alpha} \triangleq \frac{\alpha}{2}$  and  $\bar{Z} \triangleq (\bar{Z} \nu)^2$ . Equation (14) implies that  $\kappa_2 = \phi_0 \triangleq \frac{\alpha \mu}{2} L$ , highlighting its dependence on the parameters  $\alpha$ ,  $\mu$ , and  $L$ .

In this section, we recover the result of [1] using an approximation method. The exact PDF of the sum of independent and identically distributed (i.i.d.)  $\alpha$ - $\mu$  distributed random variables is derived in [1]:

$$f_{\|\mathbf{h}\|^2}(y) = \left( \frac{\bar{\alpha} \mu^\mu}{\Gamma(\mu) \bar{Z}^{\bar{\alpha} \mu}} \right)^L \sum_{i=0}^{\infty} \frac{\delta_i y^{i \bar{\alpha} + \bar{\alpha} \mu L - 1}}{\Gamma(i \bar{\alpha} + L \mu \bar{\alpha})}, \quad (15)$$

where the coefficients  $\delta_i$  are determined as

$$\delta_i = \begin{cases} \Gamma(\bar{\alpha} \mu)^L, & i = 0 \\ \sum_{\ell=1}^i \frac{\delta_{i-\ell} (\ell L + \ell - i) \Gamma(\bar{\alpha} (\ell + \mu)) \left(-\mu \left(\frac{1}{Z}\right)^{\bar{\alpha}}\right)^\ell}{i \Gamma(\bar{\alpha} \mu) \ell!}, & i \geq 1. \end{cases} \quad (16)$$

As proposed in [12], finding the exponent  $\kappa_2$  requires approximating the PDF,  $f_{\|\mathbf{h}\|^2}(y)$ , for small values of  $y$ . For such small values  $y$  in (15), the term with the smallest exponent of  $y$  dominates the series. This corresponds to the  $i = 0$  term in the summation. Hence, the first order approximation becomes:

$$f_{\|\mathbf{h}\|^2}(y) = \left( \frac{\bar{\alpha} \mu^\mu \Gamma(\bar{\alpha} \mu)}{\Gamma(\mu) \bar{Z}^{\bar{\alpha} \mu}} \right)^L \frac{y^{\bar{\alpha} \mu L - 1}}{\Gamma(L \mu \bar{\alpha})} + o(y^{\bar{\alpha} \mu L - 1}). \quad (17)$$

Evaluating (12) for large  $\Upsilon$  results in

$$\begin{aligned} \Pr\left(\|\mathbf{h}\|^2 \leq \frac{1}{\Upsilon}\right) &= \int_0^{\frac{1}{\Upsilon}} f_{\|\mathbf{h}\|^2}(y) dy \\ &= \left( \frac{\bar{\alpha} \mu^\mu \Gamma(\bar{\alpha} \mu)}{\Gamma(\mu) \bar{Z}^{\bar{\alpha} \mu}} \right)^L \frac{\Upsilon^{-\bar{\alpha} \mu L}}{\Gamma(\bar{\alpha} \mu L + 1)} + o\left(\Upsilon^{-\bar{\alpha} \mu L}\right), \end{aligned} \quad (18)$$

where the interchange in the order of the integral and the small-o notation can be justified by the Lebesgue's dominated convergence theorem (DCT). Thus, the diversity exponent is given by  $\kappa_2 = \bar{\alpha} \mu L = \frac{\alpha \mu}{2} L$ .

##### B. The Second $\alpha$ - $\mu$ Model

We examine the THz  $\alpha$ - $\mu$  indoor channel model of (6). To derive the PDF of  $\|\mathbf{h}\|^2$  in this case, we use the result of [20] where it has been shown that

$$f_{\|\mathbf{h}\|^2}(y) \approx \sum_{m=1}^{\Psi} \frac{c_m \bar{\alpha} \bar{\beta}^{\bar{\alpha} \bar{\mu}} y^{\bar{\alpha} \bar{\mu} - 1}}{(\omega_m \bar{z})^{\bar{\alpha} \bar{\mu}} \Gamma(\bar{\mu})} e^{-\left(\bar{\beta} \frac{y}{\omega_m \bar{z}}\right)^{\bar{\alpha}}}, \quad (19)$$

where

$$\bar{\alpha} = \frac{\alpha}{2}, \quad \bar{\mu} = \sum_{i=1}^L \mu_i, \quad \bar{\beta} = \frac{\Gamma(\bar{\mu} + \frac{1}{\bar{\alpha}})}{\Gamma(\bar{\mu})}, \quad \bar{z} = \sum_{i=1}^L (\bar{x}_i \nu)^2.$$

For any arbitrary integer,  $\Psi$ , the parameters  $c_m$  and  $\omega_m$  are determined by solving the system of linear equations:

$$\sum_{m=1}^{\Psi} c_m \omega_m^n = \frac{\mathbb{E}[Z^n]}{\mathbb{E}^n[Z]} \xi^{(n)}, \quad n = 0, 1, 2, \dots, 2M - 2,$$

$$\sum_{m=1}^{\Psi} \frac{c_m}{\omega_m^{\bar{\alpha} \bar{\mu}}} = \bar{\alpha}^{L-1} \frac{\bar{z}^{\bar{\alpha} \bar{\mu}} \Gamma(\bar{\mu})}{\bar{\beta}^{\bar{\alpha} \bar{\mu}} \Gamma(\bar{\alpha} \bar{\mu})} \times \prod_{i=1}^L \frac{\beta_i^{\bar{\alpha} \mu_i} \Gamma(\bar{\alpha} \mu_i)}{\bar{y}_i^{\bar{\alpha} \mu_i} \Gamma(\mu_i)}.$$

Here,  $\xi^{(n)}$  is defined as  $\xi^{(n)} = \frac{\Gamma(\bar{\mu} + \frac{n}{\bar{\alpha}}) \Gamma^{n-1}(\bar{\mu})}{\Gamma^n(\bar{\mu} + \frac{1}{\bar{\alpha}})}$ . To derive  $\mathbb{E}[Z^n]$ , we use the following formula, which relies on the individual terms of the summation in the random variable  $Z$ :

$$\begin{aligned} E(Z^n) &= \sum_{n_1=0}^n \sum_{n_2=0}^{n_1} \dots \sum_{n_{L-1}=0}^{n_{L-2}} \binom{n}{n_1} \binom{n_1}{n_2} \dots \binom{n_{L-2}}{n_{L-1}} \\ &\quad \times E(Y_1^{n-n_1}) E(Y_2^{n_1-n_2}) \dots E(Y_L^{n_{L-1}}). \end{aligned} \quad (20)$$

We proceed next to finding  $\kappa_1$  and  $\kappa_2$  for the THz model in (6), using (19).

1) *Exact Method:* Starting with (13) and using (19), we obtain

$$\Pr_e = \sum_{m=1}^{\Psi} \frac{\Lambda_m}{2} \int_0^\infty y^{\bar{\alpha} \bar{\mu} - 1} \operatorname{erfc}\left(\frac{\sqrt{\Upsilon} y}{\sqrt{2}}\right) \exp\left(-\bar{\beta} \frac{y}{\omega_m \bar{z}}\right)^{\bar{\alpha}} dy, \quad (21)$$

where, to compute this integral, we follow the procedure outlined in [20, Eq. 30]. A step-by-step solution is provided therein for further details. As a result, we obtain:

$$\begin{aligned} \Pr_e &= \sum_{m=1}^{\Psi} \frac{\Lambda_m}{2\sqrt{\pi}} \left( \frac{Y}{2} \right)^{-\bar{\alpha} \bar{\mu}} \\ &\quad \times H_{2,2}^{1,2} \left[ \left( \frac{2\bar{\beta}}{Y \omega_m \bar{z}} \right)^{\bar{\alpha}} \middle| \begin{matrix} (1 - \bar{\alpha} \bar{\mu}, \bar{\alpha}) (\frac{1}{2} - \bar{\alpha} \bar{\mu}, \bar{\alpha}) \\ (0, 1) (-\bar{\alpha} \bar{\mu}, \bar{\alpha}) \end{matrix} \right]. \end{aligned} \quad (22)$$

For  $\Upsilon \rightarrow \infty$ , the term  $t = \left(\frac{2\bar{\beta}}{Y \omega_m \bar{z}}\right)^{\bar{\alpha}}$  in (22) approaches zero. In [11, Appendix F], the authors conducted an asymptotic

analysis of the Fox H-function  $H_{p,q}^{m,n}(t|.)$  in the regime where  $t \rightarrow 0$  to obtain

$$H_{p,q}^{m,n}(z) = \sum_{j=1}^m \left[ h_j^* z^{b_j/\beta_j} + O\left(z^{(b_j+1)/\beta_j}\right) \right] \quad (z \rightarrow 0), \quad (23)$$

$$h_j^* = \frac{\prod_{i=1, i \neq j}^p \Gamma\left(b_i - \frac{b_j \beta_i}{\beta_j}\right) \prod_{i=1}^n \Gamma\left(1 - a_i + \frac{b_j \alpha_i}{\beta_j}\right)}{\beta_j \prod_{i=n+1}^p \Gamma\left(a_i - \frac{b_j \alpha_i}{\beta_j}\right) \prod_{i=m+1}^q \Gamma\left(1 - b_i + \frac{b_j \beta_i}{\beta_j}\right)}.$$

Using the asymptotic expression (23), for  $\Upsilon \rightarrow \infty$ , equation (22) becomes

$$\Pr_{\Upsilon \rightarrow \infty} \approx \frac{2^{\bar{\alpha}\bar{\mu}-1}}{\sqrt{\pi}} \left( \sum_{m=1}^{\Psi} \Lambda_m \right) \Upsilon^{-\bar{\alpha}\bar{\mu}} \left[ h_1^* + O\left(\frac{2\bar{\beta}}{\Upsilon \omega_m \bar{z}}\right) \right]. \quad (24)$$

As observed, the diversity exponent is given by  $\kappa_2 = \bar{\alpha}\bar{\mu} = \frac{\alpha}{2} \sum_{j=1}^L \mu_j$ . This quantifies the rate at which the probability of error decreases with increasing SNR, where higher values of  $\bar{\alpha}\bar{\mu}$  imply higher diversity gains. In addition, we find  $\kappa_1 = \frac{2^{\bar{\alpha}\bar{\mu}-1}}{\sqrt{\pi}} \left( \sum_{m=1}^{\Psi} \Lambda_m \right) h_1^*$ . Our results in (24) are consistent with those reached in [2] as both methods yield the same diversity exponent.

2) *Approximation Method:* We recover  $\kappa_2$  using the approximation method. When  $y$  is sufficiently small, we use the approximation  $\exp(y) \approx 1 + o(y)$ , where (19) boils down to

$$f_{\|\mathbf{h}\|^2}(y) \approx \sum_{m=1}^{\Psi} \Lambda_m y^{\bar{\alpha}\bar{\mu}-1} + o\left(y^{\bar{\alpha}\bar{\mu}-1}\right), \quad (25)$$

where  $\Lambda_m = \frac{c_m \bar{\alpha} \bar{\beta}^{\bar{\alpha}\bar{\mu}}}{(\omega_m \bar{z})^{\bar{\alpha}\bar{\mu}} \Gamma(\bar{\mu})}$ . This implies that, for large values of  $\Upsilon$ ,

$$\Pr\left(\|\mathbf{h}\|^2 \leq \frac{1}{\Upsilon}\right) = \sum_{m=1}^{\Psi} \Lambda_m \int_0^{\frac{1}{\Upsilon}} y^{\bar{\alpha}\bar{\mu}-1} dy + \int_0^{\frac{1}{\Upsilon}} o\left(y^{\bar{\alpha}\bar{\mu}-1}\right) dy$$

$$\approx \left( \sum_{m=1}^{\Psi} \Lambda_m \right) \frac{\Upsilon^{-\bar{\alpha}\bar{\mu}}}{\bar{\alpha}\bar{\mu}} + o\left(\Upsilon^{-\bar{\alpha}\bar{\mu}}\right), \quad (26)$$

Equation (26) implies that the diversity exponent is equal to  $\kappa_2 = \bar{\alpha}\bar{\mu} = \frac{\alpha}{2} \sum_{j=1}^L \mu_j$ , which is consistent with the result of the exact method in (24).

## V. OUTDOOR DIVERSITY ANALYSIS

This section analyzes the diversity behavior in outdoor THz channels. According to [13], the probability of error for  $L$  branch MRC receiver can be expressed as

$$\Pr_e = \frac{1}{\pi} \int_0^{\pi/2} \left( \mathcal{L}\{f_{\gamma'}\} \left( \frac{g}{\sin^2 \theta} \right) \right)^L d\theta, \quad (27)$$

where  $g = 1$  for binary phase-shift keying (BPSK),  $\gamma' = \Upsilon|h|^2$ , with  $|h|^2$  defined in (9), and  $\mathcal{L}\{f_{\gamma'}\}(\cdot)$  is the Laplace transform of  $f_{\gamma'}(\cdot)$ . In Appendix A, we derive a closed-form expression of  $\mathcal{L}\{f_{\gamma'}\}(\cdot)$  and find its high SNR approximation to evaluate  $\Pr_e$  at high SNR in order to extract the corresponding diversity exponent. Using the high SNR approximation of  $\mathcal{L}\{f_{\gamma'}\}(\cdot)$  given by (A.7), we apply the multinomial expansion to the resulting sum raised to the  $L$ -th power [14], [21] to find an approximate expression of (27) for large  $\Upsilon$ :

$$\Pr_{\Upsilon \rightarrow \infty} \approx$$

$$\frac{1}{\pi} \sum_{\substack{k_1+k_2+\dots+k_N=L \\ k_1, k_2, \dots, k_N \geq 0}} \frac{L!}{k_1! k_2! \dots k_N!} \Upsilon^{-\sum_{j=1}^N k_j b_j}$$

$$\times \frac{\prod_{j=1}^N (a_j \Gamma(b_j))^{k_j}}{g^{\sum_{j=1}^N b_j k_j}} \times \int_0^{\pi/2} \left( \sin^2(\theta) \right)^{\sum_{j=1}^N b_j k_j} d\theta \quad (28)$$

$$\approx \frac{1}{\pi} \sum_{\substack{k_1+k_2+\dots+k_N=L \\ k_1, k_2, \dots, k_N \geq 0}} \frac{L!}{k_1! k_2! \dots k_N!} \Upsilon^{-\sum_{j=1}^N k_j b_j}$$

$$\times \frac{\prod_{j=1}^N (a_j \Gamma(b_j))^{k_j}}{g^{\sum_{j=1}^N b_j k_j}} 2^{\Phi-2} B\left(\frac{\Phi}{2}, \frac{\Phi}{2}\right), \quad (29)$$

where  $a_j = \alpha_j / (2\beta_j)$ ,  $b_j = \beta_j / 2$ ,  $\Phi = 2 \sum_{j=1}^N b_j k_j + 1$ , and  $B(\cdot, \cdot)$  represent the beta function which is given as  $B(x, y) = \frac{\Gamma(x+y)}{\Gamma(x)\Gamma(y)}$ , and where we used standard beta function identities [21, 3.621.1] to justify equation (29). This expansion enables us to express the error probability as a finite sum of terms that clearly expose the diversity order and its dependence on system parameters. By identification, the diversity exponent is given as  $\kappa_2 = \left(\frac{L}{2}\right) \max_{1 \leq j \leq N} \beta_j$ . For  $L = 1$ , our result exactly matches the diversity gain reported in [11], where the error probability  $\Pr_e$  is derived for the SISO case.

## VI. SIMULATION RESULTS

We validate the theoretical analysis through Monte Carlo simulations, leveraging variations of the TeraMIMO simulator, configured with parameters derived from THz channel measurements [5], [7]. We define  $N_0 = k_B T B$ , where  $k_B$  is the Boltzmann constant,  $B$  is the system bandwidth, and  $T = 300$  K is the system temperature. Simulations are performed under BPSK modulation with  $f = 0.142$  THz and  $B = 4$  GHz. The used antenna gains are  $G_r = 19$  dBi and  $G_t = 0$  dBi [18]. We adjust  $P_t$  to vary the SNR range. For indoor small-scale fading, we evaluate the  $\alpha$ - $\mu$  model from [7] with different parameters.

For THz outdoor, Fig. 3 shows bit error rate (BER) results under a MG fading for  $N = 2$ ,  $w = [0.513, 0.487]$ ,  $\beta = [3.753, 22.598]$ , and  $\zeta = [0.159, 0.054]$  [18]. The simulations consider  $L = 2, 3, 4$  diversity branches and demonstrate the adequacy of the asymptotic analysis at high SNR as captured by (29). In Fig. 4a and 4b, we plot the PDF of the MG distribution under different parameters taken from [18]. In line with  $\kappa_2 = \left(\frac{L}{2}\right) \max_{1 \leq j \leq N} \beta_j$  for MG, increasing  $\max_{1 \leq j \leq N} \beta_j$  concentrates the PDF around the LoS component (a better channel).

Figure 1a depicts the BER performance for the  $\alpha$ - $\mu$  distribution with parameters  $\alpha = 3.45388$  and  $\mu = 0.51571$ , as derived from experimental measurements in [7]. The results are shown for two diversity configurations:  $L = 3$  and  $L = 4$ . The theoretical analysis is based on the results of the exact method as captured by equation (14). The approximation method in (18) predicts the same diversity exponent  $\kappa_2$ , and its accuracy is thus captured by the plot of the exact method. The close agreement between (14) and the simulation results in the high SNR regime confirms the validity of our analysis. As anticipated, increasing the number of diversity branches  $L$  leads to significant performance improvements, highlighting the effectiveness of diversity in mitigating fading

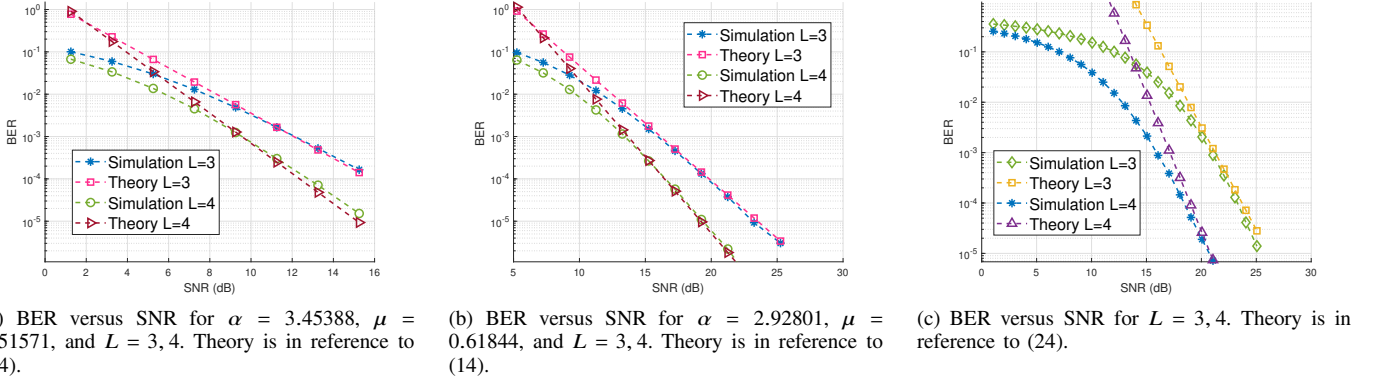


Fig. 1. Performance evaluation of BER under different  $\alpha$ - $\mu$  fading parameters and diversity orders.

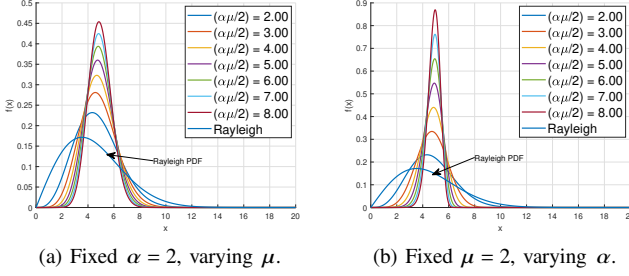


Fig. 2. PDF of the  $\alpha$ - $\mu$  distribution under two parameter conditions.

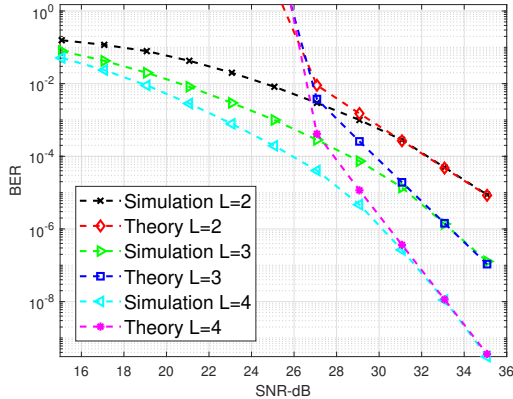


Fig. 3. BER versus SNR for MG distribution. Theory is in reference to (29).

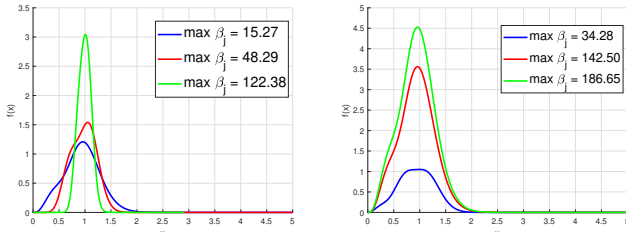


Fig. 4. PDF of MoG distribution for two different  $N$ .

effects. Fig. 1b depicts the outcome of a similar setup but for a different set of channel parameters,  $\alpha = 2.92801$  and  $\mu = 0.61844$  [7]. A third numerical example is presented in Fig. 1c where the second form of the  $\alpha$ - $\mu$  channel is

considered (6). The model parameters are taken from [7]. Once more, we observe a close match in the high SNR regime between the theoretical and simulated curves.

The decrease in  $\text{Pr}_e$  with  $\kappa_2 = \frac{\alpha\mu}{2}L$  as a function of SNR can be explained by the fact that  $\alpha$ - $\mu$  PDF becomes more concentrated as the product  $\alpha\mu$  increases. In figures 2a and 2b, we plot the  $\alpha$ - $\mu$  PDF for various values of  $\mu$  and  $\alpha$ , respectively. The figures highlight the effect of the product  $\alpha\mu$  on the density function: the greater the  $\alpha\mu$  product, the higher the concentration of the PDF around its LoS component (the better the channel), which is in line with the diversity exponent expression as captured by  $\kappa_2$ .

## VII. CONCLUSION

In this paper, we present a diversity analysis for THz communication systems in both indoor and outdoor scenarios. For the indoor case, we recover the diversity results of [1], [2] using an approximation approach and provide a new exact analysis for the generalized  $\alpha$ - $\mu$  distribution. For the outdoor scenario, we characterize the diversity behavior using the Laplace transform expression of the PDF of the squared MG distribution. The results from the simulated Monte Carlo runs show excellent agreement with the analytical expressions. Our analysis highlights the impact of the concentration characteristics of the  $\alpha$ - $\mu$  and MG distributions on diversity gain, demonstrating that tighter clustering of multipath components can enhance signal reliability in dense scattering environments. These insights provide valuable guidelines for the design of efficient and reliable THz communication systems under realistic channel conditions.

## APPENDIX A

### LAPLACE TRANSFORM OF SQUARED MIXTURE OF GAMMA

To compute the Laplace transform of the PDF of the square of MG, we follow the approach of [1, Appendix A], where the Laplace transform of the  $\alpha$ - $\mu$  PDF is derived. The proof steps presented hereafter are similar to those presented in [1]. Using (9), we write the PDF of  $\gamma' = Y|h|^2$  as

$$f_{\gamma'}(y) = \sum_{i=1}^N a_i y^{b_i-1} \exp(-c_i \sqrt{y}) \quad (\text{A.1})$$

where  $a_i = \alpha_i \Upsilon^{-b_i} / (2\nu^{\beta_i})$ ,  $b_i = \beta_i/2$ ,  $c_i = \zeta_i / (\sqrt{\Upsilon}\nu)$ . The Laplace transform for  $\Re\{s\} \geq 0$  is given by

$$\begin{aligned} \mathcal{L}\{f_{\gamma'}(y)\}(s) &= \int_0^\infty e^{-sy} f_{\gamma'}(y) dy \\ &= \sum_{i=1}^N a_i \int_0^\infty y^{b_i-1} \exp(-c_i \sqrt{y}) \exp(-sy) dy \\ &= \sum_{i=1}^N a_i \int_0^\infty y^{b_i-1} \exp(-sy) G_{0,1}^{1,0} \left[ c_i \sqrt{y} \middle| \begin{matrix} \sim \\ 0 \end{matrix} \right] dy, \end{aligned} \quad (\text{A.2})$$

where in order to write equation (A.2), the exponential function is replaced by its Meijer  $G$ -function representation

$$e^{-x} = G_{0,1}^{1,0} \left[ x \middle| \begin{matrix} \sim \\ 0 \end{matrix} \right] \quad [6].$$

Using [22, eq. (07.34.02.0001.01)] and after interchanging the order of integration, we rewrite (A.2) as

$$\begin{aligned} \mathcal{L}\{f_{\gamma'}\}(s) &= \frac{1}{2\pi j} \sum_{i=1}^N a_i \oint_{\mathfrak{L}_{s_1}} (c_i)^{-s_1} \Gamma(s_1) \\ &\quad \times \int_0^\infty \exp(-sy) y^{b_i-1-\frac{s_1}{2}} dy ds_1, \end{aligned} \quad (\text{A.3})$$

where  $s_1$  is a complex variable of integration, and  $\mathfrak{L}_{s_1}$  is a closed contour in the complex plane that encloses all the poles of  $\Gamma(s_1)$ . After evaluating the resulting inner integral in (A.3), we obtain

$$\begin{aligned} \mathcal{L}\{f_{\gamma'}\}(s) &= \frac{1}{2\pi j} \sum_{i=1}^N a_i s^{-b_i} \oint_{\mathfrak{L}_{s_1}} \Gamma(s_1) \Gamma\left(b_i - \frac{s_1}{2}\right) \left(\frac{c_i}{\sqrt{s}}\right)^{-s_1} ds_1 \\ &= \frac{1}{2\pi j} \sum_{i=1}^N a_i s^{-b_i} \oint_{\mathfrak{L}_{s_1}^\dagger} \Phi(s_1) ds_1, \end{aligned} \quad (\text{A.4})$$

where  $\Phi(s_1) = \Gamma(s_1) \Gamma\left(b_i - \frac{s_1}{2}\right) \left(\frac{c_i}{\sqrt{s}}\right)^{-s_1}$  and  $\mathfrak{L}_{s_1}^\dagger$  is a new contour that appears as the integration over  $y$  deforms  $\Phi(s_1)$ . As mentioned in [1, Appendix A], the new contour allows to represent  $\mathcal{L}\{f_{\gamma'}\}(s)$  in terms of a meromorphic function analytically defined on the strip  $0 < s_1 < b_i$  and with singularities located at  $s_1 = -t$  and  $s_1 = 2(b_i+t)$ ,  $\forall t \in \mathbb{N}_0$ . The contour  $\mathfrak{L}_{s_1}^\dagger$  is chosen to start at  $\infty + j\xi_1$  and end at  $\infty + j\xi_2$ , for  $-\infty < \xi_1 < \xi_2 < +\infty$ , in such a way that  $\mathfrak{L}_{s_1}^\dagger$  encloses all the poles of  $\Gamma(b_i - \frac{s_1}{2})$  in the positive direction. Now, using Cauchy's residue theorem, equation (A.4) can be expressed as follows [23]:

$$\mathcal{L}\{f_{\gamma'}\}(s) = \sum_{i=1}^N a_i s^{-b_i} \sum_{t=0}^\infty \text{Res}[\Phi(s_1) : \{s_1 = -t\}], \quad (\text{A.5})$$

where  $\text{Res}[\Phi(s_1) : \{s_1 = -t\}]$  is the residue of  $\Phi(s_1)$  at the poles  $s_1 = -t$ . Evaluating the residues  $\text{Res}[\Phi(s_1) : \{s_1 = -t\}] = \lim_{s_1 \rightarrow -t} (s_1 + t) \Phi(s_1)$  [23, eq. (16.3.3)], we get:

$$\mathcal{L}\{f_{\gamma'}\}(s) = \sum_{i=1}^N \frac{\alpha_i \Upsilon^{-\frac{\beta_i}{2}}}{2\nu^{\beta_i}} \cdot s^{-\frac{\beta_i}{2}} \sum_{t=0}^\infty \frac{\Gamma\left(\frac{\beta_i+t}{2}\right) \left(-\frac{\zeta_i}{\sqrt{\Upsilon}\nu\sqrt{s}}\right)^t}{t!}. \quad (\text{A.6})$$

At high values of  $\Upsilon$ , the argument of the inner series becomes increasingly small, causing the higher-order terms to decay rapidly. As a result, the series is well-approximated by its first term, with the remaining terms contributing negligibly. Thus,

we get:

$$\mathcal{L}\{f_{\gamma'}\}(s) \approx \sum_{i=1}^N \frac{\alpha_i \Upsilon^{-\frac{\beta_i}{2}} \Gamma\left(\frac{\beta_i}{2}\right)}{2\nu^{\beta_i}} \cdot s^{-\frac{\beta_i}{2}}. \quad (\text{A.7})$$

## REFERENCES

- [1] F. D. Almeida García, F. R. A. Parente, M. D. Yacoub, and J. C. S. S. Filho, "On the exact sum PDF and CDF of  $\alpha-\mu$  variates," *IEEE Transactions on Wireless Communications*, vol. 22, no. 8, pp. 5084–5095, 2023.
- [2] M. Payami and A. Falahati, "Accurate variable-order approximations to the sum of  $\alpha - \mu$  variates with application to MIMO systems," *IEEE Transactions on Wireless Communications*, vol. 20, no. 3, pp. 1612–1623, 2021.
- [3] H. Sarieddeen, M.-S. Alouini, and T. Y. Al-Naffouri, "An overview of signal processing techniques for terahertz communications," *Proc. IEEE*, vol. 109, no. 10, pp. 1628–1665, 2021.
- [4] F. Sheikh *et al.*, "THz measurements, antennas, and simulations: From the past to the future," *IEEE Journal of Microwaves*, vol. 3, no. 1, pp. 289–304, 2022.
- [5] S. Tarboush, H. Sarieddeen, H. Chen, M. H. Loukil, H. Jemaa, M.-S. Alouini, and T. Y. Al-Naffouri, "TeraMIMO: A channel simulator for wideband ultra-massive MIMO terahertz communications," *IEEE Transactions on Vehicular Technology*, vol. 70, no. 12, pp. 12325–12341, 2021.
- [6] A. B. Enad, H. Sarieddeen, J. Fahs, H. Jemaa, and T. Y. Al-Naffouri, "Performance analysis of data detection in the thz-band under channel-correlated noise," *IEEE Communications Letters*, pp. 1–1, 2025.
- [7] E. N. Papasotiriou *et al.*, "An experimentally validated fading model for THz wireless systems," *Sci. Rep.*, vol. 11, no. 1, p. 18717, 2021.
- [8] A.-A. A. Boulogeorgos, E. N. Papasotiriou, and A. Alexiou, "Analytical performance assessment of THz wireless systems," *IEEE Access*, vol. 7, pp. 11436–11453, 2019.
- [9] S. Atapattu, C. Tellambura, and H. Jiang, "A mixture gamma distribution to model the SNR of wireless channels," *IEEE Trans. Wireless Commun.*, vol. 10, no. 12, pp. 4193–4203, 2011.
- [10] J. Jung *et al.*, "Capacity and error probability analysis of diversity reception schemes over generalized- $K$  fading channels using a mixture gamma distribution," *IEEE Trans. Wireless Commun.*, vol. 13, no. 9, pp. 4721–4730, 2014.
- [11] H. Jemaa *et al.*, "Performance analysis of outdoor THz links under mixture Gamma fading with misalignment," *IEEE Commun. Lett.*, vol. 28, no. 11, pp. 2668–2672, 2024.
- [12] D. Tse and P. Viswanath, *Fundamentals of wireless communication*. Cambridge university press, 2005.
- [13] M. K. Simon and M.-S. Alouini, *Digital communication over fading channels*. John Wiley & Sons, 2005, vol. 95.
- [14] A. P. Prudnikov *et al.*, *Integrals and series: Special functions*. CRC press, 1986, vol. 2.
- [15] A. A. Kilbas, *H-transforms: Theory and Applications*. CRC press, 2004.
- [16] A. B. Enad, J. Fahs, H. Sarieddeen, H. Jemaa, and T. Y. Al-Naffouri, "Performance analysis of linear detection under noise-dependent fast-fading channels," *IEEE Signal Processing Letters*, vol. 32, pp. 2918–2922, 2025.
- [17] A. M. Magableh and M. M. Matalgah, "Moment generating function of the generalized  $\alpha-\mu$  distribution with applications," *IEEE Commun. Lett.*, vol. 13, no. 6, pp. 411–413, 2009.
- [18] E. N. Papasotiriou *et al.*, "Outdoor THz fading modeling by means of Gaussian and Gamma mixture distributions," *Sci. Rep.*, vol. 13, no. 1, p. 6385, 2023.
- [19] E. Karakoca *et al.*, "Measurement-based modeling of short range terahertz channels and their capacity analysis," in *Proc. IEEE Global Commun. Conf. (GLOBECOM)*, 2023, pp. 1471–1476.
- [20] H. Jemaa *et al.*, "Performance and complexity analysis of terahertz-band mimo detection," 2025.
- [21] I. S. Gradshteyn and I. M. Ryzhik, *Table of integrals, series, and products*. Academic press, 2014.
- [22] Wolfram Research, "Wolfram research," <http://functions.wolfram.com>, 2025, accessed: Apr. 30, 2025.
- [23] E. Kreyszig, *Advanced Engineering Mathematics*, 10th ed. Hoboken, NJ, USA: Wiley, 2010.